

# Systematic errors in direct state measurements with quantum controlled measurements

Le Bin Ho\*

*Department of Physics, Kindai University, Higashi-Osaka, 577-8502, Japan and  
Ho Chi Minh City Institute of Physics, VAST, Ho Chi Minh City, Vietnam*

(Dated: February 19, 2020)

Von Neumann measurement framework describes a dynamic interaction between a target system and a probe. In contrast, a quantum controlled measurement framework uses a qubit probe to control the actions of different operators on the target system, and convenient for establishing universal quantum computation. In this work, we use a quantum controlled measurement framework for measuring quantum states directly. We introduce two types of the quantum controlled measurement framework and investigate the systematic error (the bias between the true value and the estimated values) that caused by these types. We numerically investigate the systematic errors, evaluate the confidence region, and investigate the effect of experimental noise that arises from the imperfect detection. Our analysis has important applications in direct quantum state tomography.

## I. INTRODUCTION

Quantum state tomography (QST) is a process of getting the information of quantum states from measurement data [1]. Under the tremendous growth in quantum technologies, QST is of vital importance for benchmarking, experimentally validating quantum devices, and establishing new quantum technologies. Therefore, it induces a critical demand to develop effective schemes for the QST and evaluate their efficiency, including innovation, practically realizable, and significance.

Typically, a standard quantum state tomography (sQST) includes (i) the measurements of multiple copies of a system in a complete set of noncommuting observables, and (ii) the reconstruction of the most likely quantum state from the measured data set using efficient algorithms such as linear inversion, maximum-likelihood, least squares estimations, etc [2]. In the past years, many endeavors have been devoted to rising the efficiency of the sQST [3–6]. It is, however, particularly challenging to apply for high-dimensional systems because it requires dramatically increasing measurement cost (a full state tomography of a  $d$ -dimensional system requires at least  $d^2 - 1$  different measurements) and thus, consumes substantial calculation time. Numerous practical works have been dedicated to reducing the number of measurements, emergent with compressed sensing [7, 8], reduced density matrix [9], and adaptive quantum tomography [10]. So far, recent achievements on dynamics enhancement and dynamics control of entangled systems have been reported [11, 12], which pave the way for studying tomography of entangled systems.

Separate from the sQST, a direct state measurement (DSM) method allows for measuring the wave functions directly [13]. It was originally proposed by Lundeen et al. based on the evidence that the amplitudes of the wave functions are proportional to weak values [13]. The DSM

has more experimental merit than the sQST because it is straightforward, simple, versatile, required only local measurements [14], and also be able to apply for large systems [15–19]. It was enormously extended to general mixed states [14, 20, 21], phase-space distributions [14, 19, 22, 23], enlarged Hilbert space [24], and nonlocal entangled states, recently [25].

There are numerous reports on the improving measurement precision in the DSM using strong interaction measurements [21, 26, 27], compressive sensing [28], enlarged Hilbert space [24], and also continuous probe state [29]. Besides, examining the novelty, efficacy, and significance of the DSM had been reported [30]. The statistical error estimation [31] and the protection of the systematic errors when the probe undergoes decoherence [32] have also been focused recently.

Measurements used in the DSM typically described by a von Neumann model, which requires a dynamical interaction between a target system and a probe [33], see also [34–36] for strong interaction measurements of weak values. Recently, Ogawa et al. [37], however, has proposed a measurement framework of “probe-controlled-system transformation” that without using the von Neumann measurement. That framework actually can be derived from the von Neumann measurement, and thus they are operationally equivalent. In that framework, a target system interacts with a control qubit probe via the actions of different operators controlled by the qubit probe and can be seen as a “quantum controlled measurement” (see Sec. II A below.)

Previously, Hofmann [38] has also developed a framework of the quantum controlled measurement where the control qubit probe controls the operations of zero interaction (identity operator) or fully projective measurement on the target system. This method is a kind of quantum controlled gate, and the same procedure has been experimentally verified for measuring weak values [14, 39].

An excellent feature of the quantum controlled measurement is its applicability of the cyclic transformation property, which paves the way for using a scan-free

---

\* Electronic address: binho@kindai.ac.jp

method [15] (see discussion on Sec. IV below.) A scan-free method is that all the data after a post-selection process will be kept and used for estimating quantum states. Therefore, it will help to improve the measurement precision in the DSM.

In this work, we study the systematic errors in the DSM caused by different operational types in quantum controlled measurements. By definition, systematic error is a bias between the true value and the estimated values. We consider two types of operational interaction, i.e., type-I and type-II, correspond to Hofmann's and Ogawa's frameworks, respectively. We first analyze the systematic errors caused by these types. Then, we also compare their efficiency by evaluating the confidence region. We finally investigate the systematic errors under the imperfect detection noise, i.e., the noise that arises from the imperfection of the measuring detectors. In these calculations, we analyze the fidelity, a figure of merit that is obtained from Monte Carlo simulations.

We emphasize that type-II corresponds to an arbitrary strong interaction DSM. It thus represents the prevailing evolutions of the DSM. Whereas, the performance of type-I on the DSM has not been known yet. Therefore, it is essential to investigate and compare the efficiency of the DSM via these two types of operational quantum controlled measurement.

The structure of this paper is organized as follows. Section II introduces the measurement schemes of the DSM using two types of operational quantum controlled measurement. Section III presents the main numerical results of the systematic errors, including the investigation of the confidence region and the effect of noise. Section IV is devoted to a discussion. The paper concludes with a summary in Sec. V.

## II. DIRECT STATE MEASUREMENT WITH QUANTUM CONTROLLED INTERACTION

### A. Quantum controlled interaction

Let us first introduce a general form of quantum controlled measurement framework [37, 38]. In this framework, a target system is controlled by a control qubit probe. The interaction between the target system and the control qubit probe is given by

$$U = U_1 \otimes |0\rangle\langle 0| + U_2 \otimes |1\rangle\langle 1|, \quad (1)$$

where  $U_i$ , ( $i = 1, 2$ ) are two operators operate on the target system, and  $|0\rangle, |1\rangle$  are two bases of the control qubit probe. Such operators can be implemented in experiments if their absolute eigenvalues are smaller or equal to one [37].

We next apply the quantum controlled measurement framework to measure the quantum state directly. We consider two types of operational interaction in (1) as following.

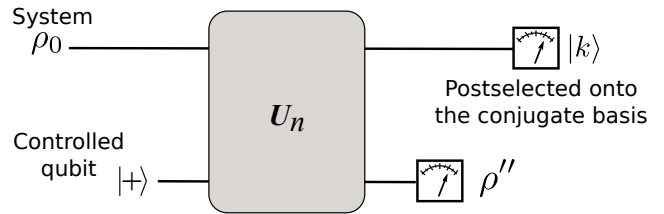


FIG. 1. (Color online.) Scheme of the direct state measurements (DSM). A control qubit probe is coupled to a target system (in  $d$ -dimensional Hilbert space) via a unitary  $U_n$ ,  $n \in [0, d-1]$ . The target system is then postselected onto the conjugate basis  $\{k\}$ , while the control qubit probe is measured on different bases, i.e.,  $\{0, 1\}$ ,  $\{+, -\}$ ,  $\{L, R\}$  to reproduce the target system state  $\rho_0$ .

### B. Type-I operational interaction

We consider a measurement scheme between a target system and a control qubit probe as schematically shown in Fig. 1. The target system is initially given in the density matrix  $\rho_0$ ,

$$\rho_0 = \sum_{n,m=0}^{d-1} \rho_{nm} |n\rangle\langle m|, \quad \text{with } \rho_{nm} = \langle n | \rho_0 | m \rangle, \quad (2)$$

an unknown state needed to be estimated,  $d$  is the dimension of the target system. The control qubit probe is initially prepared in the state  $|+\rangle$ , i.e.,  $|+\rangle = (|0\rangle + |1\rangle)/\sqrt{2}$ . The initial joint state becomes

$$\rho = \rho_0 \otimes |+\rangle\langle +|. \quad (3)$$

Let us consider the interaction is an invert quantum controlled gate which we name as type-I operational interaction:

$$U_n = I_s \otimes |0\rangle\langle 0| + |n\rangle\langle n| \otimes |1\rangle\langle 1|, \quad (4)$$

where  $I_s$  is a  $d$ -dimensional identity matrix in the target system space. Note that this interaction is similar to Hofmann's and can be implemented in optics where the control qubit probe is a polarized single photon [38]. This kind of implementation has been reported in [14, 39].

After the interaction, the joint state becomes

$$\rho' = U_n \rho U_n^\dagger. \quad (5)$$

The target system is then postselected onto a conjugate basis  $|k\rangle = \frac{1}{\sqrt{d}} \sum_{m=0}^{d-1} e^{i2\pi mk/d} |m\rangle$ , while the remaining control qubit state is given by

$$\rho'' = \langle k | \rho' | k \rangle = \begin{pmatrix} \rho''_{00}(n, k) & \rho''_{01}(n, k) \\ \rho''_{10}(n, k) & \rho''_{11}(n, k) \end{pmatrix}. \quad (6)$$

Explicitly, we have

$$\rho''_{00}(n, k) = \frac{1}{2d} \sum_{n, m=0}^{d-1} e^{\frac{i2\pi(m-n)k}{d}} \rho_{nm}; \quad (7)$$

$$\rho''_{10}(n, k) = \frac{1}{2d} \sum_{m=0}^{d-1} e^{\frac{i2\pi(m-n)k}{d}} \rho_{nm}; \quad (8)$$

$$\rho''_{01}(n, k) = \rho''_{10}(n, k)^*; \text{ and} \quad (9)$$

$$\rho''_{11}(n, k) = \frac{1}{2d} \rho_{nn}. \quad (10)$$

Using the Fourier transformation, we obtain

$$\rho_{nm} \propto 2d \sum_k e^{\frac{i2\pi(n-m)k}{d}} \rho''_{10}(n, k). \quad (11)$$

Then, the element  $\rho_{nm}$  is calculated from the measurement result of  $\rho''_{10}(n, k)$  in the control qubit probe. To obtain  $\rho''_{10}(n, k)$ , we measure the control qubit probe in different bases:

$$\rho''_{10}(n, k) = \frac{1}{2} \left[ (P_+ - P_-) + i(P_L - P_R) \right], \quad (12)$$

where  $P_j = \text{tr}[|j\rangle\langle j|\rho'']$  is the probability when measuring the control qubit probe in different bases; where  $|j\rangle \in \{|0\rangle, |1\rangle\}, \{|+\rangle, |-\rangle\}, \{|L\rangle, |R\rangle\}$ , where  $|\pm\rangle = \frac{1}{\sqrt{2}}(|0\rangle \pm |1\rangle)$ ,  $|L\rangle = \frac{1}{\sqrt{2}}(|0\rangle + i|1\rangle)$ ,  $|R\rangle = \frac{1}{\sqrt{2}}(|0\rangle - i|1\rangle)$ .

### C. Type-II operational interaction

We consider an arbitrary coupling between the target system and the control qubit probe. The initial joint state is the same as (3) in Sec. II B. The interaction is given by

$$\mathbf{U}_n = \left( \mathbf{I}_s - \varepsilon_\theta |n\rangle\langle n| \right) \otimes |0\rangle\langle 0| + \sin \theta |n\rangle\langle n| \otimes |1\rangle\langle 1|, \quad (13)$$

which we name as type-II operational interaction. Here  $\varepsilon_\theta \equiv 2 \sin^2 \frac{\theta}{2}$ , and  $\theta$  is the coupling strength. For  $\theta \ll 1$ , the measurement is said to be weak. For  $\theta = \pi/2$ , the measurement is strong, while  $\theta < \pi/2$  corresponds to an arbitrary strength measurement. This type is equivalent to an arbitrary strong von Neumann measurement framework [26, 27, 40–44], such that, as we can see in the von Neumann measurement, a unitary interaction is given by

$$\begin{aligned} \mathbf{U}_n^{\text{vNm}} &= e^{-i\theta |n\rangle\langle n| \otimes \sigma_y} \\ &= \mathbf{I}_{\text{sp}} - |n\rangle\langle n| \otimes [(1 - \cos \theta) \mathbf{I}_p + i \sin \theta \sigma_y], \end{aligned} \quad (14)$$

where  $\mathbf{I}_{\text{sp}} = \mathbf{I}_s \otimes \mathbf{I}_p$ ;  $\mathbf{I}_s, \mathbf{I}_p$  are identity matrices in the target system and control qubit probe, respectively. vNm stands for ‘‘von Neumann measurement.’’ The action of  $\mathbf{U}_n^{\text{vNm}}$  on the control qubit probe initially prepared in state  $|0\rangle$  leads to

$$(\mathbf{I}_s - \varepsilon_\theta |n\rangle\langle n|) \otimes |0\rangle\langle 0| + \sin \theta |n\rangle\langle n| \otimes |1\rangle\langle 1|, \quad (15)$$

which is the same as (13) above. This type of measurement covers all of the versions of DSM from strong [26, 27] to weak interaction [40–42] by changing the coupling strength. This method also includes the coupling-deformed-pointer method, which is an arbitrary strong interaction [43, 44].

Next, after the interaction given in (13) and the post-selection onto the conjugate basis  $|k\rangle$ , the final control qubit state ( $\rho''$ ) is given as in (6). Then, we have

$$\begin{aligned} \rho''_{00}(n, k) &= \frac{1}{2d} \left[ \sum_{n, m=0}^{d-1} e^{\frac{i2\pi(m-n)k}{d}} \rho_{nm} \right. \\ &\quad \left. - \varepsilon_\theta \left( \sum_{m=0}^{d-1} e^{\frac{i2\pi(m-n)k}{d}} \rho_{nm} + c.c \right) + \varepsilon_\theta^2 \rho_{nn} \right]; \end{aligned} \quad (16)$$

$$\rho''_{10}(n, k) = \frac{\sin \theta}{2d} \left[ \sum_{m=0}^{d-1} e^{\frac{i2\pi(m-n)k}{d}} \rho_{nm} + \varepsilon_\theta \rho_{nn} \right]; \quad (17)$$

$$\rho''_{01}(n, k) = \rho''_{10}(n, k)^*; \text{ and} \quad (18)$$

$$\rho''_{11}(n, k) = \frac{1}{2d} \sin^2 \theta \rho_{nn}. \quad (19)$$

It is now possible to calculate the element  $\rho_{nm}$  by using the Fourier transformation:

$$\rho_{nm} \propto 2d \tan \frac{\theta}{2} \delta_{nm} \rho''_{11}(n, k) + \sum_k e^{\frac{i2\pi(n-m)k}{d}} \rho''_{10}(n, k), \quad (20)$$

where  $\delta_{nm}$  is the Dirac delta. For a weak measurement (small  $\theta$ ), the reconstructed state is given by

$$\rho_{nm}^{\text{W}} \propto \sum_k e^{\frac{i2\pi(n-m)k}{d}} \rho''_{10}(n, k). \quad (21)$$

The same as Sec. II B, to obtain  $\rho''_{10}(n, k)$  and  $\rho''_{11}(n, k)$ , we measure the control qubit probe as follows:

$$\rho''_{10}(n, k) = \frac{1}{2} \left[ (P_+ - P_-) + i(P_L - P_R) \right], \text{ and} \quad (22)$$

$$\rho''_{11}(n, k) = P_1, \quad (23)$$

where  $P_1 = \text{tr}[|1\rangle\langle 1|\rho'']$ . Equations (20, 21) are equivalent to those derived by von Neumann measurement in [26]. This Neumann framework has been widely explored and investigated theoretically and experientially [26, 27].

Such an element matrix  $\rho_{nm}$  in Eqs. (11, 20) is given without any approximation. However, we emphasize that its obtained value depends on the experiments and the methods (that we use to measure the final control qubit state): by using different types of equipment or different methods, we have different values of  $\rho_{nm}$ , which is the main leaven of systematic errors. So far, there are various methods in the DSM, including compressive sensing method [28], enlarged Hilbert space [24], and continuous probe state [29]. However, in this work, we restrict ourselves to quantum controlled measurement framework since it includes the arbitrary strong interaction and is experimentally realizable [27, 37].

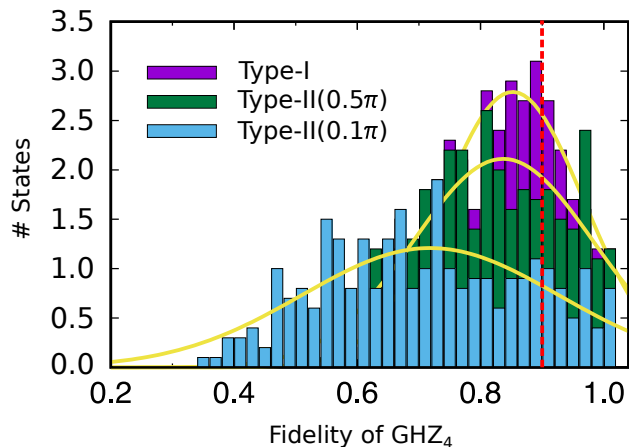


FIG. 2. (Color online.) Histogram of the fidelities estimated from 500 independent reconstructed states  $|\text{GHZ}_4\rangle$ . For each state,  $N_c = 400$  measurement repetitions have been carried out. The red-dotted line is the reference fidelity  $f_0$ . The average fidelities obtained from type-I (purple), type-II( $0.5\pi$ ) (green), and type-II( $0.1\pi$ ) (cyan) are smaller than  $f_0$ , which called systematic errors. Yellow curves are fit Gaussian.

### III. ACCURACY IN THE DSM

#### A. Random vs systematic errors

To avoid any confusion, we define random and systematic errors as following. Random error describes fluctuations around the true value that caused by unknown and unpredictable changes during the measurement process. It is essentially unavoidable but can be effectively reduced by repeating the measurement many times. Differently, systematic error is a bias between the true value and the estimated value [45]. It is raised by inaccuracy of equipment or by different measurement methods (models), such as the offset error, the scale factor error. For example, if you are using a thermometer that has not been set to zero beforehand, there will have a systematic error in measuring the temperature (offset error); or using a stretched-out measuring tape will cause a scale-factor type systematic error. In our case, the systematic error is caused by different types in the quantum controlled measurement framework.

We numerically investigate the systematic errors in the DSM caused by two types of operational interaction in Sec. II. We first consider a four-qubit GHZ state  $|\text{GHZ}_4\rangle = 1/\sqrt{2}(|0000\rangle + |1111\rangle)$  as a target state (later, we also examine other common states such as W state and Dicke state.) We also assume the state is mixed with small white noise that  $\rho_0 = (1-p)|\text{GHZ}_4\rangle\langle\text{GHZ}_4| + p\mathbf{I}_s/16$ . We choose  $p$  so that the reference fidelity  $f_0 \equiv \langle\text{GHZ}_4|\rho_0|\text{GHZ}_4\rangle = 0.9$ . To reconstruct the state, we perform the Monte Carlo simulations with the cumulative method [24, 40]. Our code can be found in [46]. To analyze the systematic errors, we compare the bias between the reference fidelity and average fidelities obtained

from type-I and type-II as follows.

Figure 2 shows the histogram of the estimated fidelity  $f(\rho_r) = \langle\text{GHZ}_4|\rho_r|\text{GHZ}_4\rangle$ , where  $\rho_r$  is the estimated density state, obtained from (11) or (20). Note that this fidelity is compared with the GHZ state, so that its exact value is  $f_0 = 0.9$ , as we fit above. If we compare  $\rho_r$  with  $\rho_0$  then the exact value of the fidelity should be one. The reason we shift the exact value to 0.9 is that for the illustration purpose, as we can see from Fig. 2. From the histogram, we can calculate the average fidelity ( $f_{\text{ave}}$ ), which is the average value of  $f(\rho_r)$ 's; and the standard deviation ( $\delta f$ ), which stands for the random error.

On one hand, the standard deviation ( $\delta f$ ) obtained from type-I is  $\pm 0.115$ , while those ones for type-II( $\theta$ ) with  $\theta = 0.5\pi$  and  $\theta = 0.1\pi$  are  $\pm 0.146$  and  $\pm 0.208$ , respectively. [Note that hereafter we add a suffix ( $\theta$ ) to “type-II” to declare the  $\theta$ -dependence of this type.] Among these cases, the random error of type-I is smallest while that value of type-II gradually increases when reducing the interaction strength  $\theta$ . These results are in agreement with [26].

On the other hand, the average fidelities obtained from these three cases above are 0.852, 0.837, and 0.718, respectively. These average fidelities are smaller and deviate systematically from the true value (0.9), which are known as the systematic errors [47]. To evaluate a “measure” of systematic error, we define a bias factor, which is the ratio between the reference fidelity  $f_0$  and the average fidelity  $f_{\text{ave}}$  as

$$\Delta f = \frac{f_0 - f_{\text{ave}}}{f_0}, \quad (24)$$

where  $f_0 - f_{\text{ave}}$  is an infidelity. If the bias vanishes ( $\Delta f = 0$ ), there is no systematic error at all. The larger the bias, the larger the systematic error. The analytical expression of (24) can be derived in terms of the initial unknown state. However, we emphasize that such an expression is given in an ideal case, such as the number of measurements is infinity. In this paper, we thus restrict ourselves to numerical simulation of (24), which can be served as testbed before carrying out real experiments.

As we can see from Fig. 2, the bias is small for type-I, while it gradually increases for type-II( $\theta$ ) when  $\theta$  gradually reduces from strong to weak interactions. These results are obtained after 400 measurement runs ( $N_c = 400$ ) for each  $\rho_{nm}$  and 500 estimated states to get the histogram.

While random errors can be reduced when increasing the number of copies  $N_c$ , systematic errors cannot be completely eliminated in the same way. However, the bias  $\Delta f$  can be reduced when increasing  $N_c$ , for example, see [47]; or in a general procedure called “calibration.” Hereafter, let us investigate the dependence of fidelities on  $N_c$ . The results are shown in the upper row of Fig. 3 for several initial states, including the GHZ state  $|\text{GHZ}_4\rangle$ , the W state  $|\text{W}_4\rangle$ , and the Dicke state  $|\text{D}_4^1\rangle$ . For each case, we show the average fidelities with respect to the target state for type-I (purple), type-II( $0.5\pi$ )(green),

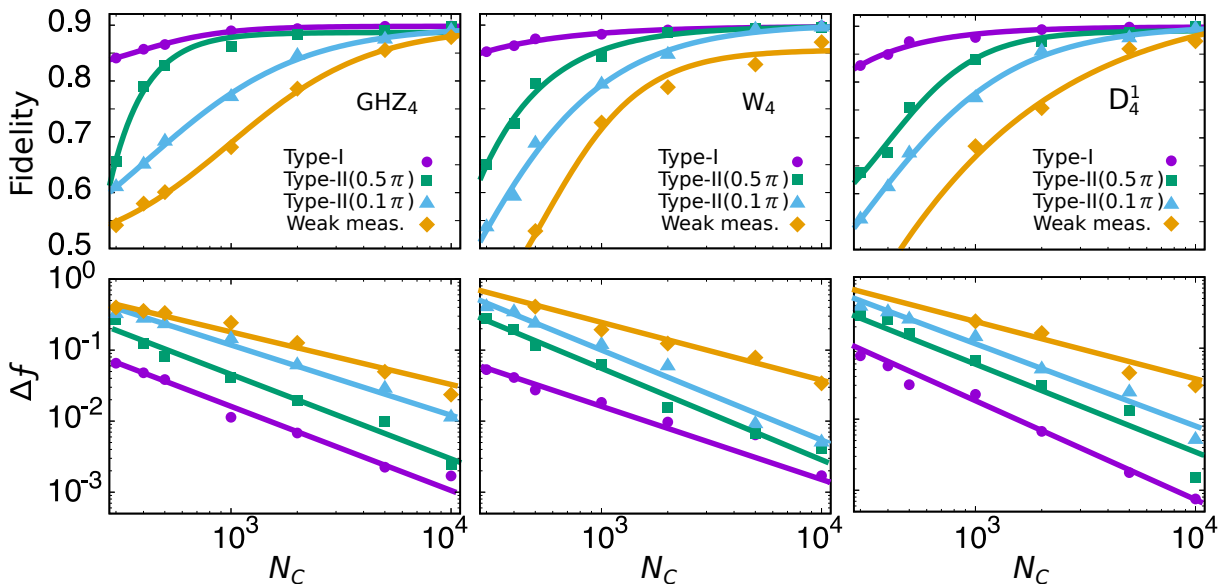


FIG. 3. (Color online.) Upper panels: The average fidelities with respect to the target state as functions of the number of copies  $N_c$  for different target states  $\text{GHZ}_4$ ,  $W_4$ , and  $D_4^1$  from left to right. For each panel, we consider different methods, ranging from type-I to type-II( $\theta$ ) and weak measurements. Lower panels: the corresponding  $\Delta f$ 's. The solid lines are the guide's eyes.

type-II( $0.1\pi$ ) (cyan), and weak measurement (orange). The results show that these fidelities depend significantly on the number of measurement copies  $N_c$  and increase with increasing  $N_c$ . Correspondingly, the biases  $\Delta f$  decrease with increasing  $N_c$ , as can be seen from the lower panels of Fig. 3. The results also suggest that the biases still remain and do not collapse between different methods when increasing  $N_c$ , which imply that the systematic errors cannot be completely eliminated. It can be seen that the systematic error is small for type-I, and it gradually increases for type-II( $\theta$ ) when  $\theta$  reduces from strong to weak interactions. We also compare to the weak measurement case, where the interaction strength is infinitely small. The results reveal that the systematic error in this case is the largest (among those methods that we are considering in this paper.) This conclusion is in agreement with previous studies [26, 40], where the bias caused by the infinitely small  $\theta$ .

Furthermore, the systematic errors also vary with the number of qubits  $N_q$ . In Fig. 4 upper panels, we show the average fidelities with respect to the target state of different methods versus  $N_q$  for different target states. We also show the corresponding biases in its lower panels. Here, we fit  $N_c = 10^5$ . The results suggest that the fidelities decrease when increasing  $N_q$  while the biases are increasing, which imply the increase in systematic errors. Similarly as above, for type-I, the systematic deviation is small while it gradually increases for type-II( $\theta$ ) when  $\theta$  reduces from strong to weak interactions. Here we omit the weak measurement case since its systematic deviation is relatively large.

## B. Confidence region

Now, let us analyze the confidence region in the DSM. Following the method of Christandl and Renner [48], we consider a region  $R_{f(\rho_r)}$  is a set of state  $\rho_r$  so that its fidelity  $f(\rho_r)$  satisfies a concrete condition

$$R_{f(\rho_r)} = \{\rho_r : \bar{f} \leq f(\rho_r) \leq 2f_0 - \bar{f} \leq 1\}, \quad (25)$$

where  $\bar{f}$  is a fixed threshold fidelity. The distribution function of  $f$  for all  $\rho_r$  is also defined as [49]

$$\mu(f) = \int_{\forall \rho_r} d\rho_r P(\rho_r) \delta[f(\rho_r) - f], \quad (26)$$

where  $P(\rho_r)$  is the normalized probability that the obtained state is  $\rho_r$ , and  $\delta[\cdot]$  is the Dirac delta. In the region  $R_{f(\rho_r)}$ , the distribution function is satisfied [48, 49]:

$$\int_{\bar{f}}^{\min\{2f_0 - \bar{f}, 1\}} \mu(f) df \geq 1 - \frac{\epsilon}{2c}, \quad (27)$$

where  $1 - \epsilon$  is the confidence level and  $c \equiv \text{poly}(N_c) = (N_c + 1)^{d-1}$ . Then, there exists a confidence region  $R_{f(\rho_r)}^\lambda$  such that

$$R_{f(\rho_r)}^\lambda = \{\rho_r : \exists \rho'_r \in R_{f(\rho_r)} \text{ with } F(\rho_r, \rho'_r) \geq 1 - \lambda^2\}, \quad (28)$$

where  $F(\rho_r, \rho'_r) = \text{tr} \sqrt{\sqrt{\rho_r} \rho'_r \sqrt{\rho_r}}$  the fidelity of the closeness between  $\rho_r$  and  $\rho'_r$ , and  $\lambda^2 = \frac{2}{N_c} (\ln \frac{2}{\epsilon} + 2 \ln c)$ . Then,

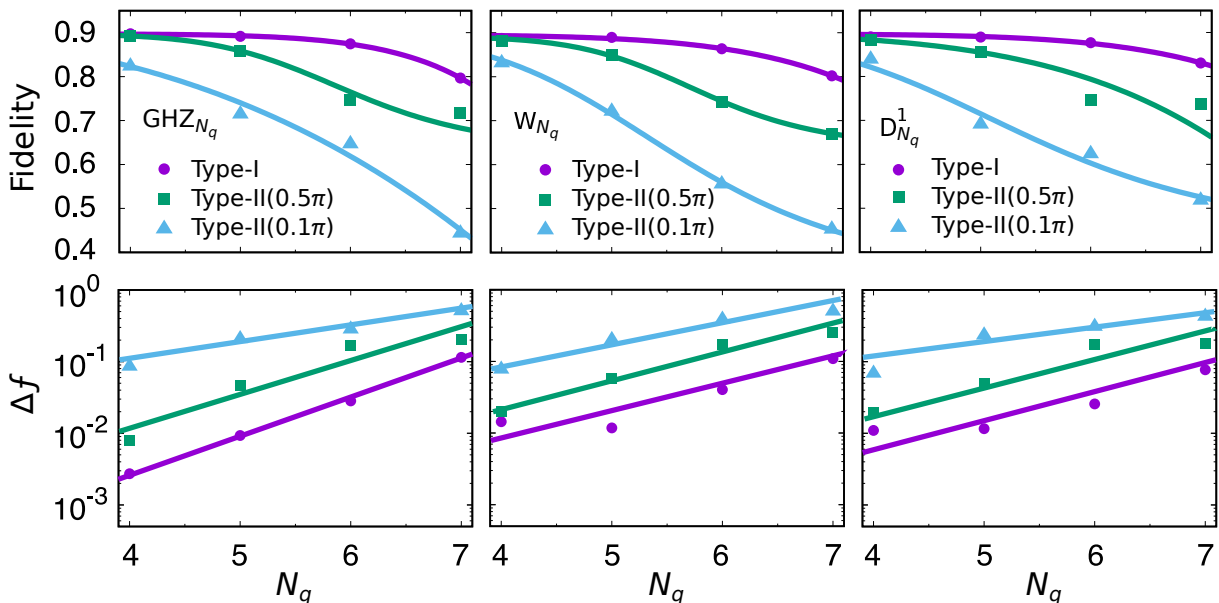


FIG. 4. (Color online.) Upper panels: The average fidelities with respect to the target state as functions of the number of qubits  $N_q$  for different target states  $\text{GHZ}_4$ ,  $W_4$ , and  $D_4^1$ . Other denotations are the same as Fig. 3. Lower panels: the corresponding  $\Delta f$ 's.

the probability that  $\rho_r$  belongs to the confidence region is given by

$$P[\rho_r \in R_{f(\rho_r)}^\lambda] \geq 1 - \epsilon. \quad (29)$$

Next, let us provide a concrete example of how to choose the confidence region priorly. Let us assume the distribution function  $\mu(f)$  is a Gaussian mean  $f_0$ :

$$\mu(f) = \frac{1}{\sqrt{2\pi\sigma^2}} e^{-\frac{(f-f_0)^2}{2\sigma^2}}, \quad (30)$$

where we choose priorly  $\sigma = \epsilon = 0.005$ , i.e., the confidence level is  $1 - 0.005 = 0.995$ . Inversely solving (27) we obtain  $\bar{f} \approx 0.858128$ . We also calculate  $\lambda^2$  and then obtain the confidence region bounded by

$$\bar{f} - \lambda^2 \leq R_{f(\rho_r)}^\lambda \leq \min(2f_0 - \bar{f} + \lambda^2, 1). \quad (31)$$

For example, with  $\text{GHZ}_4$ ,  $N_c = 10^4$ , we have  $\lambda^2 \approx 0.056461$ , then the confidence region is  $[0.801667 : 0.998333]$ , which is the yellow region in Fig. 5(b).

In Fig. 5 (a), we numerically show the ratio into percentage between the number of states  $\rho_r$  that belong to the confidence region  $R_{f(\rho_r)}^\lambda$  and all states with the confidence level at 0.995. We investigate three cases of type-I, type-II(0.5 $\pi$ ) and type-II(0.1 $\pi$ ) for several  $N_c$ . The results show that the ratio into percentage increases as  $N_c$  increases; and type-I always shows the highest percent while that one for type-II gradually decreases from strong to weak interactions.

In Fig. 5 (b), we show the histogram of these three cases where we can see that type-I lies inside the confidence region with the highest percentage.

### C. Systematic errors against the noise

In this subsection, we investigate the systematic errors under the effect of noise caused by the imperfect detection. In this case, the probability when measuring the control qubit probe ( $P_j$ ) has some noises. We consider the noise a Gaussian type [50, 51], then the probability is given as

$$P_j^{(\eta)} = \sum_{j'} \mathcal{N} e^{-\frac{(j-j')^2}{2\eta^2}} P_{j'}, \quad (32)$$

where  $\mathcal{N}$  is the normalizing factor, and  $\eta$  is the noise parameter. Physically, the imperfect detection noise means that when measuring the control qubit probe in basic  $|j\rangle$ , there is a small probability that it becomes  $|j'\rangle$  for  $j$  and  $j'$  are in  $\{|0\rangle, |1\rangle\}$ ,  $\{|+\rangle, |-\rangle\}$ , and  $\{|L\rangle, |R\rangle\}$ .

We show, in Fig. 6, the numerical results for the average fidelity of  $\text{GHZ}_4$  for two cases of type-I and type-II (0.5 $\pi$ ). It can be seen that the fidelity is protected in the case of type-I, which implies that its systematic error does not increase when increasing the noise. Meanwhile, the fidelity of type-II(0.5 $\pi$ ) rapidly drops when the noise  $\eta$  reaches around 0.3.

## IV. DISCUSSION

In our study, we show a higher accuracy for type-I operational interaction in comparison with type-II from strong to weak interactions. It can be understood because in type-I, we only measure  $\rho''_{10}(n, k)$  [equation (12)] while in the latter case, it also requires to measure

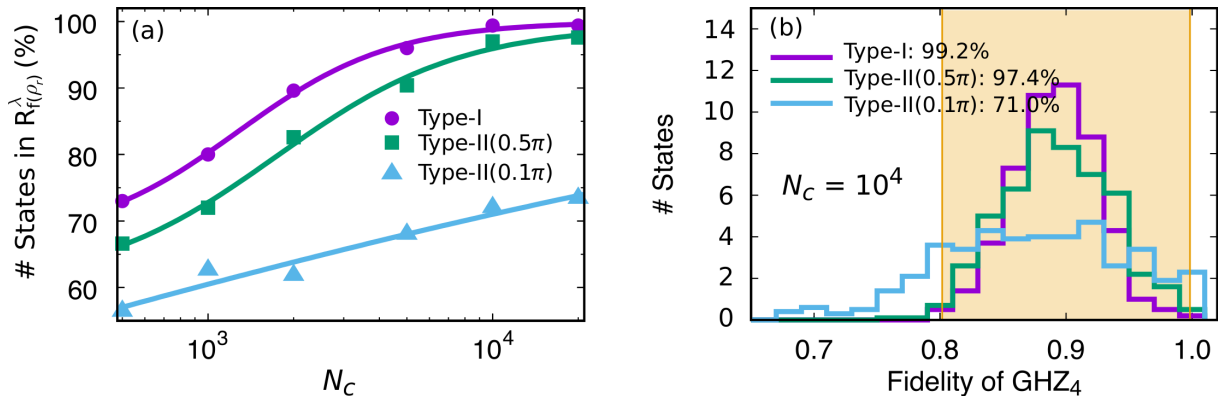


FIG. 5. (Color online.) (a) Plot of the ratio into percentage between the number of states inside the confidence region and all states. We plot for three cases shown in the figure. (b) The histogram of these three cases at  $N_c = 10^4$ . The ratios into percentages are given in the figure, while the highlight region represents the confidence region.

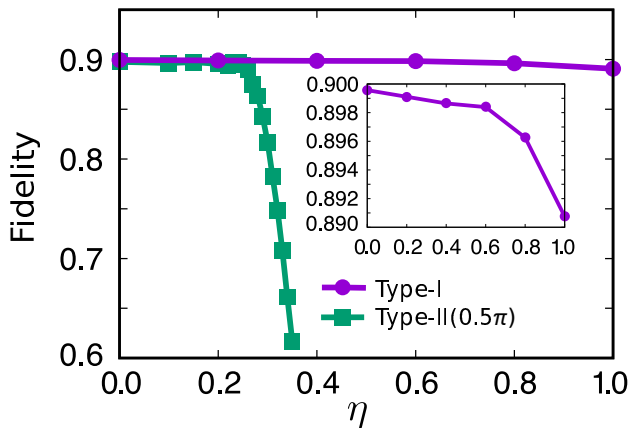


FIG. 6. (Color online.) Plot of average fidelities of GHZ<sub>4</sub> at  $N_c = 10^4$  for two cases: type-I and type-II(0.5 $\pi$ ). Inset: plot of the fidelity of type-I on a large scale.

$\rho''_{11}(n, k)$  [equations (22,23)]. Consequently, type-I gives more accuracy. Both cases of type-I and weak measurement only require the measurement of  $\rho''_{10}(n, k)$ . However, for the weak measurement case, the bias is rising due to the infinitely small of the interaction strength. As a result, the accuracy of the weak measurement case is poor.

So far, the quantum controlled interaction presents a cyclic property between pre-selected state  $|n\rangle$ , and post-selected state  $|k\rangle$ , which allows for applying the scan-free method [37]. In the scan-free method, the projection operator  $|n\rangle\langle n|$  in (4) and (13) is replaced by  $|k\rangle\langle k|$ , and the postselection is  $|n\rangle$ . We can keep all the data of the postselection  $|n\rangle$  (scan-free) that will be used in the reconstruction process. It thus gives better accuracy for the DSM [15, 37].

Furthermore, the study of confidence region is crucially important not only in theory but also in experiments because it helps to design and evaluate experiments. For example, it allows experimenters to predict the confidence

region of quantum states in advance before carrying out the experiments. Thus, the measurement time can be reduced by focusing on the confidence region. So far, the analysis of the confidence region has been carried out for the standard quantum state tomography [48, 49, 52, 53]. However, this is the first time we apply this analysis on the DSM.

## V. CONCLUSION

We have investigated the systematic operational errors in the direct state measurements (DSM) with a quantum controlled interaction framework. In this DSM scheme, a target system is controlled by a qubit probe and post-selected onto a conjugate basis; the outcomes of the control qubit probe can be measured and taken out of the estimated state. We have considered two types of operational interaction: (i) invert quantum controlled interaction (type-I) and (ii) arbitrary strong interaction (type-II), which is equivalent to a von Neumann interaction.

Our numerical results first show that type-I operational interaction gives lower systematic error than type-II, which means more accuracy. For the same confidence level, type-I has a higher ratio into percentage in the confidence region. The systematic error in type-I is also well against the noise as its fidelity is protected under the noise. These results can be explained by the difference in these two interaction types, where type-I requires fewer measurements than type-II.

Our study gives a better solution for quantum state tomography using the quantum controlled measurement scheme (better than conventional strong measurements and weak measurements.) Furthermore, its measurement is simple and applicable to high-dimension systems. This method, thus, could be a potential candidate for further characterizing the properties of large systems.

## VI. ACKNOWLEDGMENTS

We acknowledge Y. Kondo for the careful reading of the manuscript. This work was supported by JSPS KAKENHI Grant Number 19K14620.

- 
- [1] M. Paris and J. Řeháček (Eds), *Quantum State Estimation*, Lecture Notes in Physics, Vol. 649 (Springer-Verlag, Berlin Heidelberg, 2004).
- [2] K. Banaszek, G. M. D’Ariano, M. G. A. Paris, and M. F. Sacchi, *Phys. Rev. A* **61**, 010304 (1999).
- [3] H. Kosaka, T. Inagaki, Y. Rikitake, H. Imamura, Y. Mitsumori, and K. Edamatsu, *Nature* **457**, 702 (2009).
- [4] M. R. Vanner, J. Hofer, G. D. Cole, and M. Aspelmeyer, *Nature Communications* **4**, 2295 (2013).
- [5] D. Lu, T. Xin, N. Yu, Z. Ji, J. Chen, G. Long, J. Baugh, X. Peng, B. Zeng, and R. Laflamme, *Phys. Rev. Lett.* **116**, 230501 (2016).
- [6] C. H. Baldwin, I. H. Deutsch, and A. Kalev, *Phys. Rev. A* **93**, 052105 (2016).
- [7] D. Gross, Y.-K. Liu, S. T. Flammia, S. Becker, and J. Eisert, *Phys. Rev. Lett.* **105**, 150401 (2010).
- [8] S. T. Flammia, D. Gross, Y.-K. Liu, and J. Eisert, *New Journal of Physics* **14**, 095022 (2012).
- [9] T. Xin, D. Lu, J. Klassen, N. Yu, Z. Ji, J. Chen, X. Ma, G. Long, B. Zeng, and R. Laflamme, *Phys. Rev. Lett.* **118**, 020401 (2017).
- [10] G. I. Struchalin, E. V. Kovlakov, S. S. Straupe, and S. P. Kulik, *Phys. Rev. A* **98**, 032330 (2018).
- [11] M. S. Ateto, *International Journal of Quantum Information* **13**, 1550034 (2015), <https://doi.org/10.1142/S0219749915500343>.
- [12] M. S. Ateto, *Quantum Information Processing* **16**, 267 (2017).
- [13] J. S. Lundeen, B. Sutherland, A. Patel, C. Stewart, and C. Bamber, *Nature* **474**, 188 (2011).
- [14] J. S. Lundeen and C. Bamber, *Phys. Rev. Lett.* **108**, 070402 (2012).
- [15] Z. Shi, M. Mirhosseini, J. Margiewicz, M. Malik, F. Rivera, Z. Zhu, and R. W. Boyd, *Optica* **2**, 388 (2015).
- [16] M. Mirhosseini, O. S. Magaña Loaiza, S. M. Hashemi Rafsanjani, and R. W. Boyd, *Phys. Rev. Lett.* **113**, 090402 (2014).
- [17] M. Malik, M. Mirhosseini, M. P. J. Lavery, J. Leach, M. J. Padgett, and R. W. Boyd, *Nature Communications* **5**, 3115 (2014).
- [18] E. Bolduc, G. Gariepy, and J. Leach, *Nature Communications* **7**, 10439 (2016).
- [19] S. H. Knarr, D. J. Lum, J. Schneeloch, and J. C. Howell, *Phys. Rev. A* **98**, 023854 (2018).
- [20] G. S. Thekkadath, L. Giner, Y. Chalich, M. J. Horton, J. Banker, and J. S. Lundeen, *Phys. Rev. Lett.* **117**, 120401 (2016).
- [21] L. Calderaro, G. Foletto, D. Dequal, P. Villoresi, and G. Vallone, *Phys. Rev. Lett.* **121**, 230501 (2018).
- [22] J. Fischbach and M. Freyberger, *Phys. Rev. A* **86**, 052110 (2012).
- [23] M. A. de Gosson and S. M. de Gosson, *Journal of Physics A: Mathematical and Theoretical* **45**, 115305 (2012).
- [24] L. B. Ho, *Physics Letters A* **383**, 289 (2019).
- [25] W.-W. Pan, X.-Y. Xu, Y. Kedem, Q.-Q. Wang, Z. Chen, M. Jan, K. Sun, J.-S. Xu, Y.-J. Han, C.-F. Li, and G.-C. Guo, *Phys. Rev. Lett.* **123**, 150402 (2019).
- [26] G. Vallone and D. Dequal, *Phys. Rev. Lett.* **116**, 040502 (2016).
- [27] T. Denkmayr, H. Geppert, H. Lemmel, M. Waegell, J. Dressel, Y. Hasegawa, and S. Sponar, *Phys. Rev. Lett.* **118**, 010402 (2017).
- [28] X. Chen, H.-Y. Dai, L. Yang, and M. Zhang, *Phys. Rev. A* **97**, 032120 (2018).
- [29] X. Zhu and Q. Wei, *Ann. of Phys.* **376**, 283 (2017).
- [30] J. A. Gross, N. Dangniam, C. Ferrie, and C. M. Caves, *Phys. Rev. A* **92**, 062133 (2015).
- [31] I. Sainz and A. B. Klimov, *EPL (Europhysics Lett.)* **116**, 10002 (2016).
- [32] S. Pang, J. R. G. Alonso, T. A. Brun, and A. N. Jordan, *Phys. Rev. A* **94**, 012329 (2016).
- [33] J. von Neumann, *Mathematical Foundations of Quantum Mechanics: New Edition* (Princeton University Press, 2018).
- [34] E. Cohen and E. Pollak, *Phys. Rev. A* **98**, 042112 (2018).
- [35] A. Botero, *Quantum Studies: Mathematics and Foundations* **5**, 423 (2015).
- [36] T. Denkmayr, J. Dressel, H. Geppert-Kleinrath, Y. Hasegawa, and S. Sponar, *Phys. B: Cond. Mat.* **551**, 339 (2018), the 11th International Conference on Neutron Scattering (ICNS 2017).
- [37] K. Ogawa, O. Yasuhiko, H. Kobayashi, T. Nakanishi, and A. Tomita, *New Jour. of Phys.* **21**, 043013 (2019).
- [38] H. F. Hofmann, *New Journal of Physics* **16**, 063056 (2014).
- [39] C. Bamber and J. S. Lundeen, *Phys. Rev. Lett.* **112**, 070405 (2014).
- [40] L. Maccone and C. C. Rusconi, *Phys. Rev. A* **89**, 022122 (2014).
- [41] E. Haapasalo, P. Lahti, and J. Schultz, *Phys. Rev. A* **84**, 052107 (2011).
- [42] X. Chen, H.-Y. Dai, and M. Zhang, *Phys. Lett. A* **381**, 3161 (2017).
- [43] Y.-X. Zhang, S. Wu, and Z.-B. Chen, *Phys. Rev. A* **93**, 032128 (2016).
- [44] X. Zhu, Y.-X. Zhang, and S. Wu, *Phys. Rev. A* **93**, 062304 (2016).
- [45] J. Durkee, in *Management of Industrial Cleaning Technology and Process* edited by J. Durkee (Elsevier Science, Oxford, 2006) pp. 191 – 256.
- [46] L. B. Ho, “dsm-developers: A Fortran90 code for simulating the direct state measurements. <https://github.com/echkon/dsm-developers>,” <https://github.com/echkon/dsm-developers>.
- [47] C. Schwemmer, L. Knips, D. Richart, H. Wein- (2012), T. Moroder, M. Kleinmann, and O. Gühne, *Phys. Rev. Lett.* **114**, 080403 (2015).

- [48] M. Christandl and R. Renner, Phys. Rev. Lett. **109**, 120403 (2012).
- [49] P. Faist and R. Renner, Phys. Rev. Lett. **117**, 010404 (2016).
- [50] L. Pezzé and A. Smerzi, Phys. Rev. Lett. **110**, 163604 (2013).
- [51] M. Gabrielli, L. Pezzè, and A. Smerzi, Phys. Rev. Lett. **115**, 163002 (2015).
- [52] J. Wang, V. B. Scholz, and R. Renner, Phys. Rev. Lett. **122**, 190401 (2019).
- [53] J. Shang, H. K. Ng, A. Sehwat, X. Li, and B.-G. Englert, New Journal of Physics **15**, 123026 (2013).